Two-dimensional surface band structure of operating light emitting devices

R. Shikler, T. Meoded, N. Fried, B. Mishori, and Y. Rosenwaks[a)]
Department of Physical Electronics, Faculty of Engineering, Tel-Aviv University, Ramat-Aviv 69978, Israel

(Received 1 December 1998; accepted 30 March 1999)

We report on measurements of two-dimensional potential distribution with nanometer spatial resolution of operating light emitting diodes. By measuring the contact potential difference between an atomic force microscope tip and the cleaved surface of the light emitting diode, we were able to measure the device surface potential distribution. These measurements enable us to accurately locate the metallurgical junction of the light emitting device, and to measure the dependence of the built-in voltage on applied external bias. As the device is forward biased, the junction built-in voltage decreases up to flat band conditions, and then inverted. It is shown that the potential distribution across the *pn* junction is governed by self-absorption of the sub-bandgap diode emission. © *1999 American Institute of Physics.* [S0021-8979(99)07113-3]

I. INTRODUCTION

As characteristic dimensions of semiconductor devices continue to shrink, the ability to characterize structure and electronic properties in such devices at the nanometer scale has come to be of outstanding importance. A combination of scanning Kelvin force microscopy (KFM) and atomic force microscopy (AFM) has already been demonstrated as a powerful tool for conducting such measurements. Due to its promise of high-spatial-resolution surface potential measurements, the KFM has found many diverse applications in just a few years. Nonenmacher *et al.* have applied the technique to materials work function mapping.[1] Kikukawa *et al.* have conducted surface potential measurements of silicon *pn* junctions,[2] and Vatel and Tanimoto have demonstrated potential measurements of resistors,[3] and *n-i-p-i* heterostructures.[4] Although KFM has proved to be effective in electrical characterization of devices, to date there are only a few reports[5] of potential profiles of operating semiconductor devices. Such measurements provide the ability to image the surface band structure of the device in operating conditions. This ability, which has not been available up to now in the submicrometer scale, is of great interest both from physical and technological points of view. For example, it is important for understanding the relation between the device performance and its surface potential. Since band bending at the surface, affects carrier recombination[6] and breakdown phenomena, such measurements may prove to be very useful for improving performance and preventing failure in surface rich devices.

In this work, we report on measurements of two-dimensional (2D) potential distribution of operating GaP light emitting diodes (LEDs) at equilibrium and under applied bias. Measurements conducted at equilibrium (when the external forward bias is zero) enabled us to extract the location of the metallurgical junction of the device. When forward bias is applied, the junction built-in voltage at the surface (V_{bi}^{s}) decreases with increasing applied forward bias up to flat-band conditions, and then inverted. Additional measurements, including surface photovoltage spectroscopy (SPS), show that the potential distribution is governed by self-absorption of the sub-bandgap light emission from the device.

The next section describes the theory underlying the contact potential difference (CPD) measurement and the experimental setup. Section III describes and discusses the results obtained for the LED under equilibrium and nonequilibrium conditions; the results are summarized in Sec. IV.

II. KELVIN FORCE MICROSCOPY

A. Principle of the KFM method

The electrostatic force, F, on a conductive AFM tip held close to a conducting surface is given by

$$F=-\frac{V^2}{2}\frac{\partial C}{\partial z}, \tag{1}$$

where V is the potential difference between the tip and the surface, C is the capacitance between the tip and the sample, and z is the tip-sample distance. When an alternating voltage with amplitude V_1 and frequency ω is applied to the tip, the potential difference V becomes

$$V=(V_{\mathrm{CPD}}\pm V_{ext})+V_1\sin(\omega t), \tag{2}$$

where V_{CPD} is the contact potential difference between the tip and the sample given by

$$V_{\mathrm{CPD}}=\frac{\phi_{\mathrm{tip}}-\phi_{\mathrm{sample}}}{-e}, \tag{3}$$

where ϕ_{tip} and ϕ_{sample} are the tip and sample work functions, respectively, and e is the electron charge. The external potential, V_{ext}, is an additional voltage that is applied either to the tip or to the sample; the sign in front of V_{ext} is explained below.

The amplitude of the tip vibration, A, is proportional to the force F. Substituting the expression of the voltage given

a)Electronic mail: yossir@post.tau.ac.il

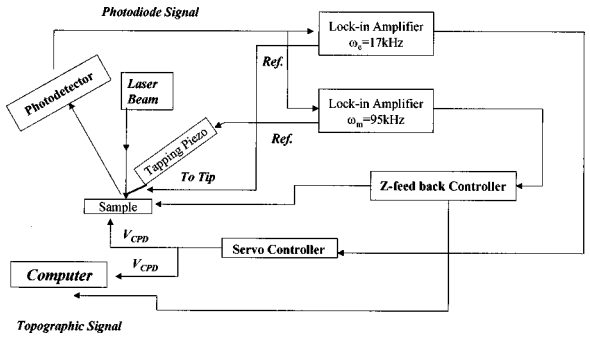

FIG. 1. Schematic diagram of the KFM measurement setup.

in Eq. (2) in Eq. (1) and collecting the terms according to their frequencies, the following form for the amplitude of the tip vibration is obtained:

$$A = S\left\{ (V_{\mathrm{CPD}} \pm V_{\mathrm{ext}})^2 + 2(V_{\mathrm{CPD}} \pm V_{\mathrm{ext}}) V_1 \sin(\omega t) + \frac{V_1^2}{2}[1 - \cos(2\omega t)] \right\}. \tag{4}$$

where S is a proportionality coefficient. Note that the amplitude of the vibration of the tip at the frequency ω is proportional to $V_1(V_{\mathrm{CPD}} \pm V_{\mathrm{ext}})$. The contact potential difference, V_{CPD}, is obtained by the following procedure: the direct current (dc) voltage, V_{ext}, is varied until the alternating current (ac) vibration of the tip at the frequency ω is nullified; at this voltage $V_{\mathrm{ext}} = \pm V_{\mathrm{CPD}}$. When the external voltage is applied to the tip or to the sample it changes their work functions. Hence, based on Eq. (3) the sign of V_{CPD} will be different in the two cases. The posteriori dc voltage difference V_{CPD}^p is thus given for the two cases as

$$V_{\mathrm{CPD}}^p = -\frac{\phi_{\mathrm{tip}}}{e} - \left(\frac{\phi_{\mathrm{sample}}}{-e} + V_{\mathrm{ext}} \right) = V_{\mathrm{CPD}} - V_{\mathrm{ext}}, \tag{5a}$$

$$V_{\mathrm{CPD}}^p = -\frac{\phi_{\mathrm{tip}}}{e} - \frac{\phi_{\mathrm{sample}}}{-e} + V_{\mathrm{ext}} = V_{\mathrm{CPD}} + V_{\mathrm{ext}}, \tag{5b}$$

where Eqs. (5a) and (5b) are for the cases of voltage applied to the sample and the tip, respectively. After the nullifying procedure, i.e., when $V_{\mathrm{CPD}}^p = 0$, we obtain $V_{\mathrm{ext}} = \pm V_{\mathrm{CPD}}$, where the ''+'' and ''−'' refer to the external bias applied to the sample and the tip, respectively. This is demonstrated in Sec. III B.

B. Experimental setup

Figure 1 shows a schematic diagram of the KFM measurement setup. It is based on a commercial AFM (Autoprobe CP, Park Scientific Instruments, Inc.) operating in noncontact mode. For topographic imaging, the cantilever, heavily doped silicon with sharpened tip (<20 nm radius), was driven by a piezoelectric bimorph at a frequency slightly above resonance.[7] An alternating voltage $V_1 \sin(\omega t)$ at a frequency of around 20 kHz was applied to the cantilever in order to induce an electrostatic force between the tip and the sample. The CPD between the tip and the sample surface was measured in the conventional way[1] by nullifying the

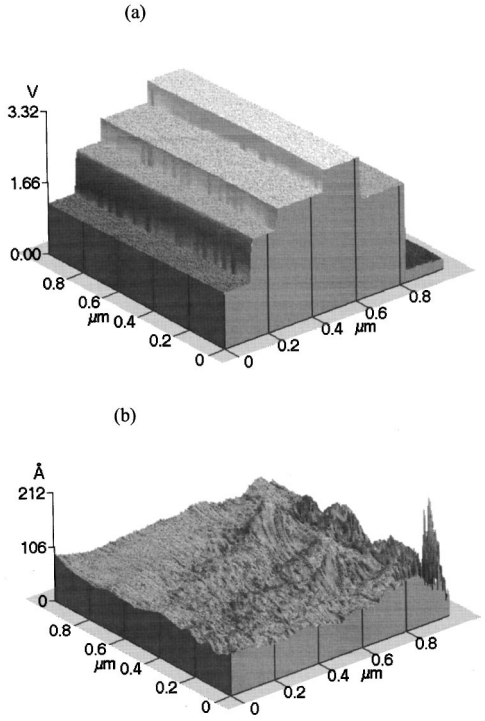

FIG. 2. (a) CPD and (b) topographic images of a thin gold layer under different applied external voltages.

output signal of a lock-in amplifier (LIA) which measures the electrostatic force at the frequency ω (see Sec. II A). The sensitivity of the surface potential measurements was evaluated by applying an external step voltage to the sample and measuring the CPD between the tip and the sample during a line scan. A sensitivity of less than 10 mV was achieved at an applied V_1 of 5 V. The measured CPD was independent of the following parameters:

(a) The amplitude of the ac bias applied to the tip (V_1), as long as it was below 5 V.
(b) The frequency of the applied ac bias, as long as it was above 15 kHz, but not close to the resonant frequency of the vibrating cantilever.
(c) The distance between the vibrating tip and the sample surface which was usually on the order of 10–20 nm.

In order to measure the accuracy of the measured CPD between the tip and the sample, and to verify that there is no ''crosstalk'' between the electrostatic and topographic signals, we have conducted the following measurement. A tunable external dc voltage was applied to a gold surface (100 nm thick gold evaporated on glass) during a two dimensional AFM scan. Figure 2 shows (a) the CPD and (b) the topographic images measured simultaneously. The changes observed in the CPD image correspond exactly to the changes in the external bias. While the changes in the applied dc voltage were abrupt and of large amplitude (3 V) the topography image did not change during the entire scan.

The GaP LED samples (grown by Elma Inc.[8]) were grown by liquid phase epitaxy. They consisted of ten μm thick Zn, doped GaP ($p \simeq 5 \times 10^{17}$ cm^{-3}) layer on top of a 40 μm thick, S-doped ($n \simeq 1 \times 10^{17}$cm^{-3}), n-type layer

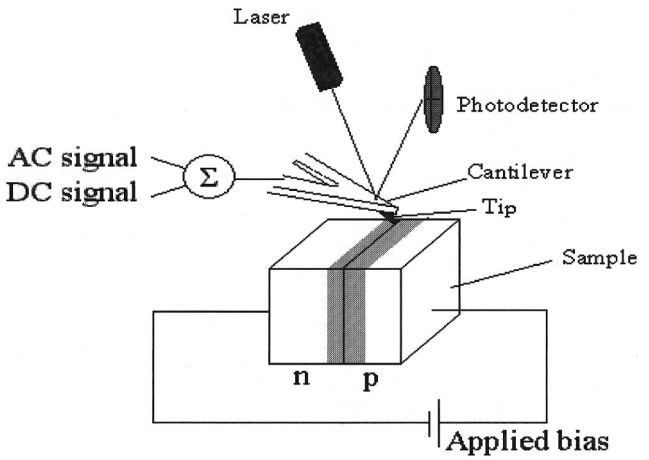

FIG. 3. Schematic of the cleaved GaP sample measurement setup under external forward bias.

grown on a GaP *n*-type substrate. The LED peak emission was at a wavelength of 565 nm. Ohmic contacts were formed using evaporation of Ni/Ga/Au/Ni/Au (Ref. 9) for the *n*-type substrate, and Pd/Zn/Pd for the top *p*-layer.[10–12] The sample was cleaved in air, and then placed in a specially designed holder for the cross-sectional KFM measurements. The bias to the LED was applied as shown in Fig. 3. Surface photovoltage measurements were carried out using a Kelvin probe unit (Besocke Delta Phi, Jülich, Germany) made of a semitransparent 2.5 mm diameter Au grid. The sample was illuminated through the grid by a light from a 250 W tungsten-halogen lamp passing through a 0.25 m grating monochromator (Oriel, USA). More details about the SPS experimental setup can be found elsewhere.[13]

III. RESULTS AND DISCUSSION

A. *p-n* junction in equilibrium

Figure 4 shows (a) the CPD and (b) the topographic images of the GaP LED in equilibrium, i.e., with no applied external voltage. The figure shows three main results:

(1) The junction potential is homogeneous throughout the scanning range (5 μm).
(2) There is no correlation between the CPD and topography images; this is in agreement with the results obtained for the gold sample in Sec. II B.
(3) The built-in potential on the surface, $V_{\mathrm{bi}}^{s} \simeq 1.1$ V; this voltage is much smaller than the value in the bulk which was calculated to be $V_{\mathrm{bi}}^{b} = 2$ V. This difference is due to surface band bending effects as will be explained in more detail below.

Figure 5(a) shows one potential line scan across the LED *pn* junction. An analysis of an abrupt *pn* junction[14] shows that the junction built-in electric field, $E = -\partial V/\partial x$, has an extremum at the metallurgical junction between the *p*-type and the *n*-type regions. Figure 5(b) shows the derivative of the measured potential with respect to the *x* axis; the *x* direction is perpendicular to the junction, i.e., parallel to the surface, as shown in the figure. It is observed that the metallurgical junction can be located with an error of less than 50

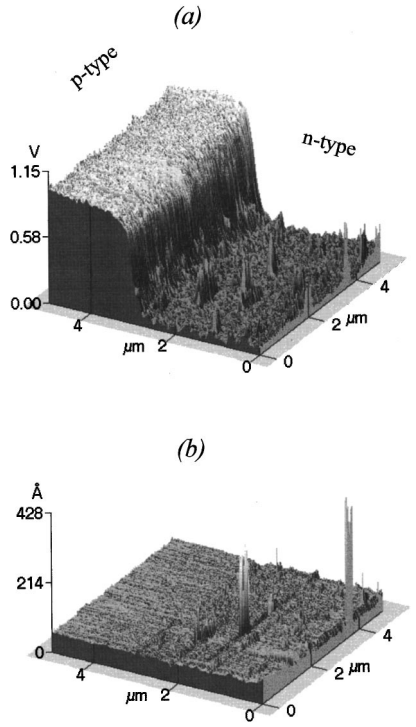

FIG. 4. (a) CPD and (b) topography images of a cleaved GaP *pn* junction under equilibrium conditions.

nm. The width of the junction can also be estimated from Fig. 5(b) to be $\simeq 0.5$ μm. This calculated width is around an order of magnitude larger compared with that calculated based on the bulk doping concentration. This inconsistency

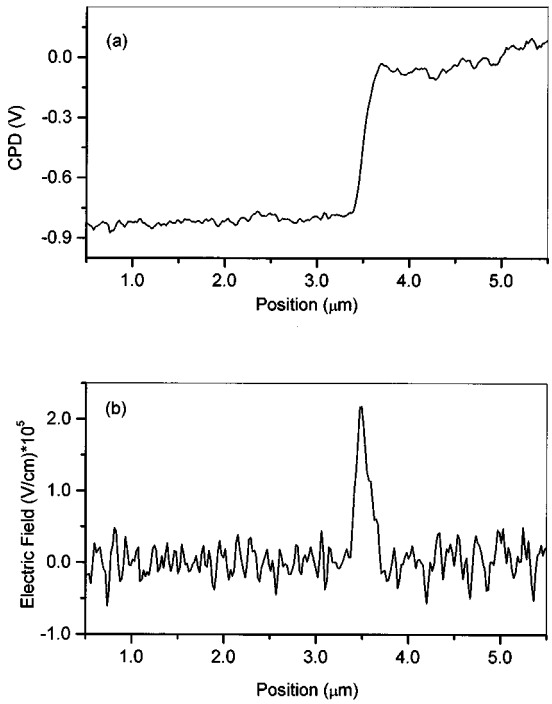

FIG. 5. (a) Measured junction potential with (b) its first derivative with respect to the *x* axis. The first derivative represents the calculated junction electric field.

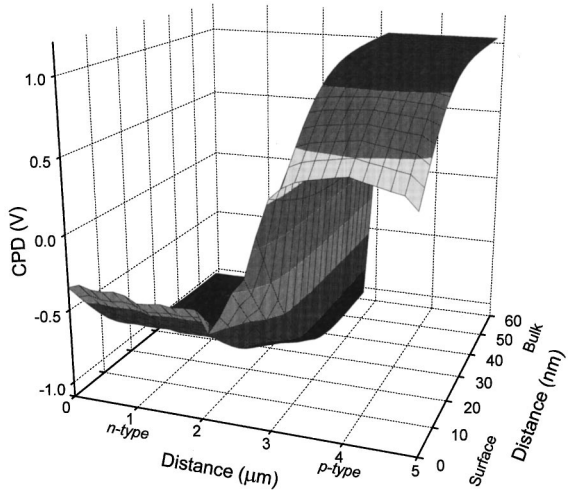

FIG. 6. Calculation of 2D potential distribution assuming symmetric depletion at the *p*- and *n*-type surface. The figure demonstrates the reduced surface built-in voltage, V_{bi}^{s}, relative to that in the bulk.

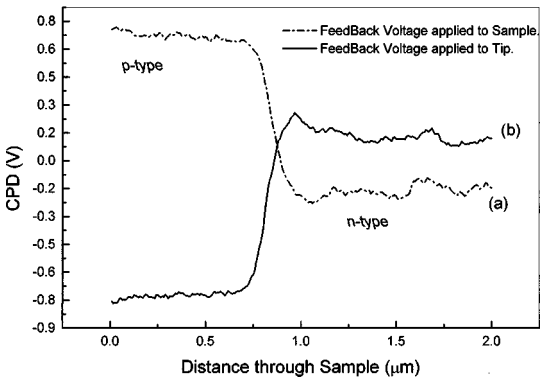

FIG. 7. Junction potential measured by applying the feedback voltage (a) to the tip, and (b) to the sample. The curves represent (a) the correct, and (b) incorrect CPD values, respectively.

is related to the difference between the built-in voltage on the surface and in the bulk and is explained in Sec. III B.

The lower V_{bi}^{s} (compared with V_{bi}^{b}) is most probably due to two main reasons: semiconductor surface states, and/or external charge on the sample surface. Surface states (due to imperfect cleavage and/or oxides on the air exposed sample) can trap holes (electrons) on the cleaved surfaces of the *p (n)* sides of the junction, creating depletion-type band bending opposite in sign on each side of the junction. Thus the bands will bend up in the *n*-doped region and down in the *p*-doped region, with the net result being a reduction of V_{bi}^{s}. The reduction of the built-in voltage on the surface may be used to derive the surface band bending and/or the surface charge on the cleaved crystal. However, the surface states distribution on the cleaved junction surface is not known and therefore the band bending can only be estimated as described below.

Figure 6 shows the 2D potential distribution calculated using Poisson's equation of the form

$$\frac{\partial^2 \phi}{\partial x^2}+\frac{\partial^2 \phi}{\partial y^2}=\frac{q}{\epsilon}(n_i e^{\phi/V_T}-n_i e^{-\phi/V_T}-D), \tag{6}$$

where ϕ is the electrostatic potential, ϵ is the permittivity of GaP, D is the net concentration of the ionized impurities (dopants), and y is the direction perpendicular to the surface. The first two terms on the right-hand side are the mobile electron and hole densities, respectively, calculated using Boltzmann's statistics, and V_T is the thermal voltage. The following boundary conditions were used to solve Eq. (6): For the x axis, Newmann's boundary conditions of the form $\partial\phi/\partial x=0$ were used. The Newmann's boundary conditions are justified far from the junction (at a distance of more than 1 μm) because the potential is constant in the direction perpendicular to the junction. The value of ϕ on the cleaved surface and at the bulk was used for the two remaining boundary conditions in the perpendicular y axis. The potential in the bulk was calculated using a one-dimensional Poisson's equation with the doping values given in Sec. II. For the surface potential (the fourth boundary condition), we have used the experimental CPD data. However, these data represent the distribution of the contact potential difference between the tip and the sample surface. Hence, the value of ϕ at the surface is known up to an arbitrary constant. For the calculation shown in Fig. 6, we assumed that the band bending at the surface was of the same magnitude (and opposite sign) for both the *n*-type and *p*-type sides.

The Poisson equation was solved using an algorithm used by Mayergoyz.[15] The result shown in Fig. 6 demonstrates that the low V_{bi}^{s} (1.1 V) relative to V_{bi}^{b} (2 V) is due to surface band bending effects as explained above. In addition, the width of the space charge region (SCR) can be obtained. Figure 6 shows that the width of the SCR in the bulk is on the order of 30 nm. This value does not change much even if the band bending at the surface is not of the same magnitude for the *p* and *n* sides and therefore, can be assumed to be the correct value. In summary, surface band bending effects cause to the difference in the magnitude of V_{bi}^{s} relative to V_{bi}^{b}.

Figure 7 shows two potential line scans across the *p*-*n* junction when the feedback (nullifying) potential is applied to (a) the sample's surface and (b) to the AFM tip. As explained in the previous section, the external voltage equals the CPD when it is applied to the sample; this is shown by curve (a) of Fig. 7. This is supported by the fact that the CPD of the *p* side of a homojunction is always higher than that of the *n* side of the junction.[2]

B. Measurements under operating conditions

Figure 8 shows CPD measurements conducted under different applied forward bias to the LED from 0 to 1.78 V. The data measured at biases of 0, 1.54, 1.62, 1.66, and 1.78 V are presented in Figs. 8 (a), 8(c)–8(e), and 8(g), respectively. Figures 8(a), 8(c)–8(e), and 8(g) present the CPD images, while Figs. 8(b), 8(f), 8(h) are the topography images. Figures 8(a)–8(b), 8(e)–8(f), and 8(g)–8(h) show that the CPD and the topography images are uncorrelated also under applied bias. The topographic images for the biases (c) and (d) are identical to these images. The most surprising phenomenon is the junction inversion obtained under forward bias of

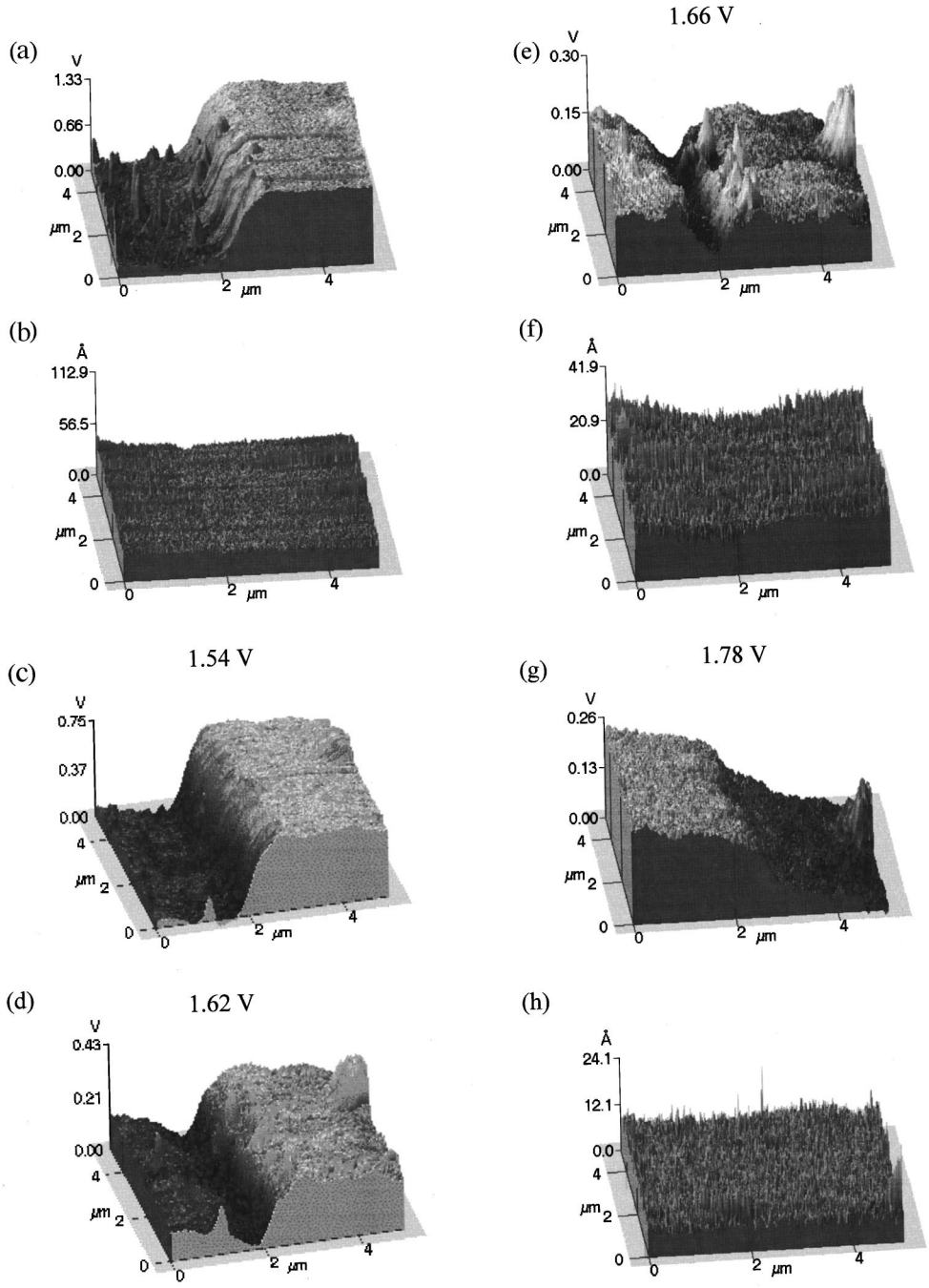

FIG. 8. CPD and topography images of the cleaved LED. Structure measured in equilibrium (a)–(b), under applied biases of (c) 1.54 V, (d) 1.62 V, (e)–(f) 1.66 V, and (g)–(h) 1.78 V. The topographic images (b), (f), and (h) demonstrate that there is no ''crosstalk'' between the van der Walls and the electrostatic forces.

1.72 V presented in Fig. 8(g); this is clearly a surface effect which cannot take place in the bulk.[14] This surface inversion implies that the junction on the surface is under reverse bias and hence, the surface current flows in opposite direction to that in the bulk.

The dependence of V_{bi}^{s} on the applied bias is summarized in Fig. 9. The figure shows nine CPD line scans measured in the range of 1.5–1.78 V external applied bias. At biases below 1.5 V, V_{bi}^{s} does not change substantially; this is because there are voltage drops on the imperfect ohmic contacts. In the 1.56 V line scan, there is a small ''valley'' that does not appear in the higher voltage line scans; this is probably an indication of surface states that change the measured CPD at this location. These surface states are not observed in

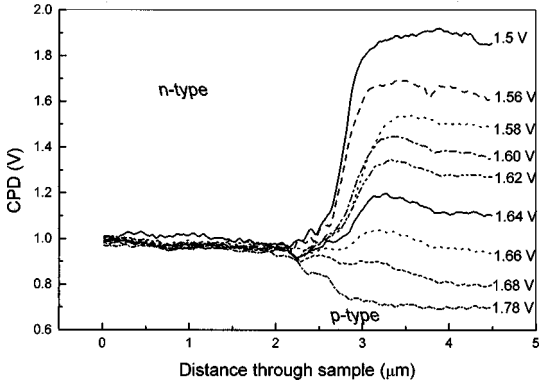

FIG. 9. Potential distribution across the *pn* junction under nine different applied forward bias.

the graphs measured under larger applied forward bias. This is attributed to light emission which populates these surface states. A similar phenomena can be observed in Figs. 8(a) and 8(c). In the range of 1.58–1.66 V, there is a voltgae ''overshoot'' on the *p*-type side of the junction. This overshoot is due to a depletion of minority carriers near the junction that increases the CPD; this is currently under further study and will be reported elswhere.

It was also found that the width of the *pn* junction does not change with decreasing surface built-in voltage. This indicates that the depletion regions width cannot be calculated based on a one-dimensional analysis; this is because the *pn* junction is measured at the surface and a two-dimensional analysis (as shown below) is required. However, the insensitivity of the junction width at the surface to V_{bi}^{s} can be explained using the following semiquantitative argument. In the one-dimensional case, the *pn* junction width depends on the ratio between the built-in voltage, V_{bi}^{s}, and the doping concentration, *D*. As will be shown in the next paragraph, there is a depletion type band bending at the *pn* junction surface. This band bending is due to surface charge opposite in sign to the ionized dopants in the two (*p* and *n*) space charge regions; thus the net charge at the surface is reduced. Therefore, the ratio between V_{bi}^{s} and D_e (the ''effective doping'' at the surface) is approximately constant. Since the depletion region width in the one-dimensional approximation is proportional to $\sqrt{V_{\mathrm{bi}}^{s}/D_e}$, it does not change with increased external applied bias.

The magnitude of V_{bi}^{s} changes by about 1.1 V in the bias range between 1.5 and 1.78 V. This large change is unexpected based on the theory of *pn* junctions;[14,16] this theory shows that V_{bi} in the bulk should decrease linearly with a proportionality factor of 1 with increasing forward bias. In principle, a change in V_{bi}^{s} which is much larger than the external applied bias can be due to two reasons: (a) Reabsorption of light emitted inside the device, (2) charging or discharging of surface states.

Changes in V_{bi}^{s} resulting from light absorption were studied using SPS. The SPS technique is based on the following principle: illumination of a semiconductor surface or interface by monochromatic light results in charge exchange between the bands and local states within the band gap. This change will be accompanied by a change in the surface potential and therefore, will change the CPD between the sample and the measuring probe. By measuring the CPD as a function of the incident light energy, a surface photovoltage spectrum like the one shown in Fig. 10 is obtained.

The figure shows SPS measurements conducted on the surface of the *p* layer. Two main transitions at 2.19 and 2.4 eV are observed. The first is a decrease of the surface photovoltage (SPV) and is due to an electron transfer from a shallow state located at an energy of $E_t = 2.19$ eV below the conduction band minimum, (E_c), to the conduction band[17] ($E_c - E_t = 2.16$ eV, the peak of LED emission energy). Such a transition increases the band bending at the *p*-layer surface (due to an increase of the free electron concentration in the conduction band), thus, decreasing V_{bi}^{s} as explained earlier. The second feature is the increase in the SPV signal at an energy around the E_g energy (2.4 eV). This increase in the CPD is due to band-to-band transition and indicates that the layer is *p* type as expected.

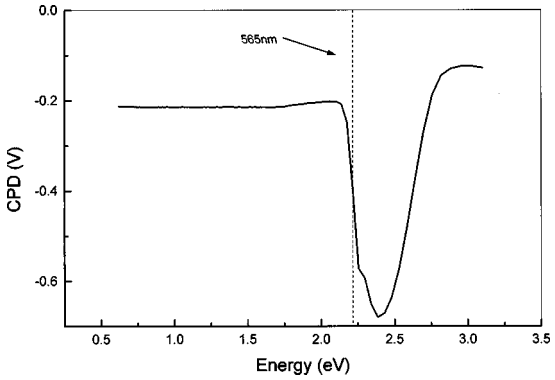

FIG. 10. Surface photovoltage spectrum (SPS) of the *p*-type Gap surface. The measurement was conducted using the standard Kelvin probe method. The vertical line represents the LED emission energy.

In order to quantify the changes in V_{bi}^{s} resulting from optical absorption, we have measured the changes in V_{bi}^{s} induced by external illumination. This was done by exciting the cleaved junction surface using argon-ion laser ($\lambda = 488$ nm) passing through an optical fiber brought to a distance of about 100 μm from the AFM tip. The photoinduced changes in V_{bi}^{s} are shown in Fig. 11. The highest light intensity $(I/I_0 = 1)$ corresponds to a photon flux of around tens of μW/cm^2 reaching the GaP surface underneath the tip. This light intensity changes V_{bi}^{s} by about 0.5 V. A similar result is observed in Fig. 12 which shows the changes in $V_{\mathrm{bi}}^{s}(|\mathrm{SPV}|)$ (right) induced by the external applied bias (the *x* axis) together with the measured emitted light intensity (left). The emitted light Intensity was measured by placing a very sensitive laser power meter (PD UV 300 Ophir Inc.) above the cleaved junction. This graph shows that a V_{bi}^{s} change of about 0.65 V is accompanied by a change of a factor of 20 in the emitted light intensity. This behavior is similar to the one obtained by the external illumination shown in Fig. 11.

In addition, the observation that $\triangle V_{\mathrm{bi}}^{s}$ changes linearly with the external applied bias supports our hypothesis that the changes in $|\mathrm{SPV}|$ are due to the absorption of the internal LED emission. This is explained in the following way: The

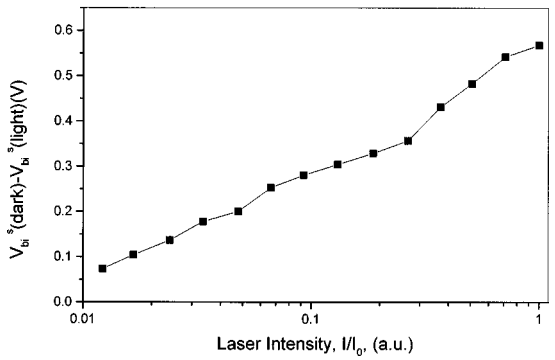

FIG. 11. Changes in the surface built in potential (V_{bi}^{s}) induced by external illumination ($\lambda = 488$ nm) as a function of normalized light intensity. The highest light intensity $(I/I_0 = 1)$ is approximately 40 μW/cm^2.

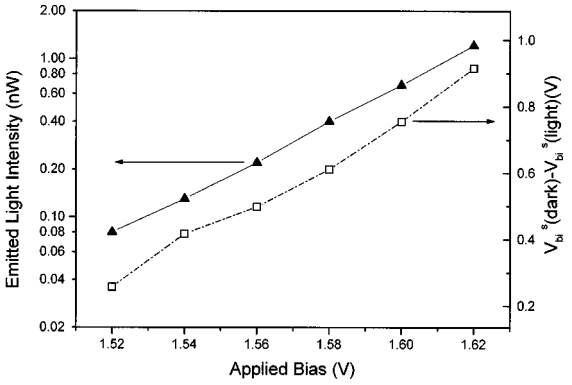

FIG. 12. Changes in V_{bi}^{s} (right), together with the measured emitted LED emission (left) as a function of the applied forward bias.

dependence of the $|\mathrm{SPV}|$ signal on light intensity is given by[18]

$$|\mathrm{SPV}| \propto \ln(L). \tag{7}$$

The measured emitted light shows an exponential dependence on the applied bias, see Fig. 11. As a result the changes in the surface built in voltage, V_{bi}^{s} have the following dependence on the applied bias:

$$V_{\mathrm{bi}}^{s} \propto \ln(L) \propto V. \tag{8}$$

Hence $V_{\mathrm{bi}}^{s}(\mathrm{dark}) - V_{\mathrm{bi}}^{s}(\mathrm{light})$ changes linearly with the applied bias V as observed in Fig. 12.

The second possibility that the changes in V_{bi}^{s} are due to changes in the surface state density is rejected due to the following argument. Under forward-applied bias, the *n*-type and *p*-type cleaved surfaces are driven into depletion as observed by the decrease of V_{bi}^{s}. Under such conditions, the minority carrier concentration at the surface increases. If these minority carriers are then trapped by surface states, the band bending on the *n* and *p* sides of the junction will decrease and cause an increase (rather than the experimentally observed decrease) of V_{bi}^{s}. Thus, we conclude that the large changes of V_{bi}^{s} and the junction reversal as a result of the applied bias, are a result of a photovoltage change induced by the LED internal emission.

The measurement of the surface band structure under operating conditions may lead to improved understanding of LED's performance in general and of indirect band gap LEDs in particular. As an example we examine the results obtained in this study. We have shown that the LED internal emission increases the band bending at the cleaved surface. This may lead to several effects:

(1) High surface reverse currents. As a result of the inverted junction on the surface, when the LED is biased in the forward direction, the junction on the surface will be under reverse bias. This will increase the device saturation current.
(2) Higher surface recombination rate. Larger surface depletion fields increase the effective recombination velocity.[19] This will decrease the device efficiency.
(3) Change of the refractive index at the surface. Large surface electric fields will change the refractive index at the surface due to the linear electroptic effect. Changes of the surface refractive index will affect the LED radiation pattern.

IV. SUMMARY

In summary, we have demonstrated the use of Kelvin force microscopy to 2D potential measurements of operating light emitting devices. The operating device surface band structure was imaged with nanometer resolution. Under forward applied bias, it was shown that the surface band structure is governed by absorption of the internal LED emission. This results in deeper depletion on the surface of the *p* side of the junction and inversion.

ACKNOWLEDGMENTS

This research is supported by the Israel Science foundation administered by the Israel Academy of Science and Humanities-Recanati and IDB group foundation, and by Grant No. 9701 of the Israel Ministry of Science. One of the authors (R.S.) is supported by Eshkol special scholarship of Israel Ministry of Science.

[1] M. Nonenmacher, M. P. O'Boyle, and H. K. Wickramasing, Appl. Phys. Lett. **58**, 2091 (1991).
[2] A. Kikukawa, S. Hosaka, and R. Imura, Appl. Phys. Lett. **66**, 3510 (1995).
[3] O. Vatel and M. Tanimoto, Appl. Phys. Lett. **77**, 2358 (1995).
[4] A. Chavez-Pirson and O. Vatel, M. Tanimoto, H. Ando, H. Iwamura, and H. Kanbe, Appl. Phys. Lett. **67**, 2358 (1995).
[5] T. Mizutani, M. Arakawa, and S. Kishimoto, IEEE Electron Device Lett. **18**, 423 (1997).
[6] C. J. Sandorf, R. N. Nottenburg, J. C. Bischoff, and R. Bhat, Appl. Phys. Lett. **51**, 33 (1987).
[7] D. Sarid and V. Elings, J. Vac. Sci. Technol. B **9**, 431 (1991).
[8] Elma Inc. 103460, Moscow, Zelenograd, Russia.
[9] K. K. Shih and J. M. Blum, Solid-State Electron. **15**, 83 (1972).
[10] T. F. Lei and G. K. Jeng, Solid-State Electron. **31**, 109 (1988).
[11] F. Zhang, Z. Song, and J. Peng, Appl. Surf. Sci. **62**, 83 (1992).
[12] F. Zhang, B. Sand, and B. Li, Appl. Surf. Sci. **78**, 71 (1994).
[13] N. Bachrach-Ashkenasy, L. Kronik, Y. Shapira, Y. Rosenwaks, M. Hanna, M. Leibovitch, and P. Ram, Appl. Phys. Lett. **68**, 879 (1996).
[14] S. M. Sze, *Physics of Semiconductor Devices, 2nd ed.* (Wiley, New York, 1985).
[15] I. D. Mayergoyz, Appl. Phys. Lett. **59**, 195 (1986).
[16] N. W. Ashcroft and N. D. Mermin, *Solid State Physics, International ed.* (Saunders College, Florida, 1976).
[17] Y. Rosenwaks, L. Burstein, Y. Shapira, and D. Huppert, Appl. Phys. Lett. **57**, 458 (1990).
[18] L. Kronik, M. Leibovitch, E. Fefer, L. Burstein, and Y. Shapira, J. Electron. Mater. **24**, 379 (1995).
[19] B. I. Bednyĭ and N. V. Baĭdus, Semiconductors **27**, 431 (1993).